THE JOURNAL OF PHYSICAL CHEMISTRY C
A JOURNAL OF THE AMERICAN CHEMICAL SOCIETY

pubs.acs.org/JPCC
Article

Exploring the Surface Segregation of Rh Dopants in PtNi Nanoparticles through Atom Probe Tomography Analysis

Se-Ho Kim,* Hosun Jun, Kyuseon Jang, Pyuck-Pa Choi, Baptiste Gault, and Chanwon Jung*

Cite This: J. Phys. Chem. C 2023, 127, 22721−22725
Read Online

ACCESS | Metrics & More | Article Recommendations | Supporting Information

ABSTRACT: Proton-exchange membrane fuel cells hold promise as energy conversion devices for hydrogen-based power generation and storage. However, the slow kinetics of oxygen reduction at the cathode imposes the need for highly active catalysts, typically Pt or Pt based, with a large available area. The scarcity of Pt increases the deployment and operational cost, driving the development of novel highly active material systems. As an alternative, a Rh-doped PtNi nanoparticle has been suggested as a promising oxygen reduction catalyst, but the three-dimensional distributions of constituent elements in the nanoparticles have remained unclear, making it difficult to guide property optimization. Here, a combination of advanced microscopy and microanalysis techniques is used to study the Rh distribution in the PtNi nanoparticles, and Rh surface segregation is revealed, even with an overall Rh content below 2 at. %. Our findings suggest that doping and surface chemistry must be carefully investigated to establish a clear link with catalytic activity that can truly be established.

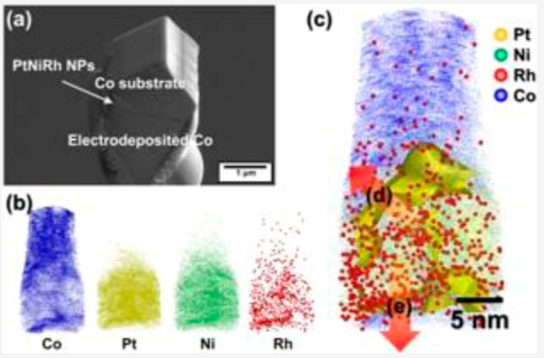

INTRODUCTION

Research on hydrogen generation is intensifying to facilitate the transition to net zero carbon emissions. Proton-exchange membrane fuel cells (PEMFCs) that convert chemical energy of hydrogen into electrical energy through hydrogen oxidation at the anode and oxygen reduction at the cathode are considered one of the future pillars of the hydrogen economy.[1,2] PEMFCs have considerable potential in transportation as a substitute for combustion engines and have already been adopted.[3] However, due to the slow reaction rate of oxygen reduction at the cathode, implementation of a large amount of Pt catalyst is unavoidable. The scarcity and cost of Pt drives a strong effort to design less expensive catalysts from earth-abundant elements while maintaining high activities.[4−7]

A common design approach to enhance catalytic activity and reduce the use of costly Pt, which in turn can modify the oxygen binding energy of the catalysts, is by alloying with transition metals such as Fe,[8,9] Co,[7,10,11] Ni,[12−15] and Mn.[16,17] For instance, Pt−Ni alloy catalysts exhibit a substantial improvement in mass activity up to a factor of 10 compared to commercial Pt/C.[4] However, it has been found that alloy systems of Pt−M nanoparticles have poor durability because the transition metal dissolves in the acidic solution under the operation condition of PEMFCs.[8−10] To address this drawback, adding a small amount of a third element, i.e., a strategy referred to as doping, has been suggested, in order to improve both durability and oxygen reduction activity. Since the successful demonstration of the Mo-doped Pt−Ni catalyst in 2015, which has shown 80 times higher catalytic activity than Pt−Ni and ∼35% improved durability,[14] research on ternary element catalysts based on Pt−Ni has been actively pursued and increasingly more complex systems are being explored, with, e.g., octonary alloys,[18,19] to further advance catalysts.

For characterization of multicomponent nanocatalysts, scanning transmission electron microscopy-energy-dispersive X-ray spectroscopy (STEM-EDS) is commonly used for elemental mapping of nanocatalysts and is increasingly complemented by atom probe tomography (APT).[20−23] APT has the ability to measure elemental distribution in three dimensions with high chemical sensitivity and subnanometer spatial resolution and as such can address issues associated with the two-dimensional projected image obtained by STEM-EDS that makes analysis of in-depth compositional distribution in three dimension (3D) challenging.[24] APT also exhibits an equal sensitivity to both light and heavy elements, whereas STEM-EDS is relatively less sensitive to light elements.[25]

Here, we analyzed Rh-doped PtNi nanoparticles that have been reported to exhibit excellent oxygen reduction activity and superior stability.[26−28] Huang et al. found that the introduction of Rh into the PtNi (111) subsurface enhances OH adsorption attributed to the ligand effect of the incorporated Rh atoms that Rh-doped PtNi nanowires exhibit

Received: July 26, 2023
Revised: October 25, 2023
Accepted: October 26, 2023
Published: November 14, 2023

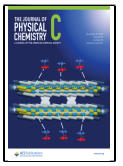

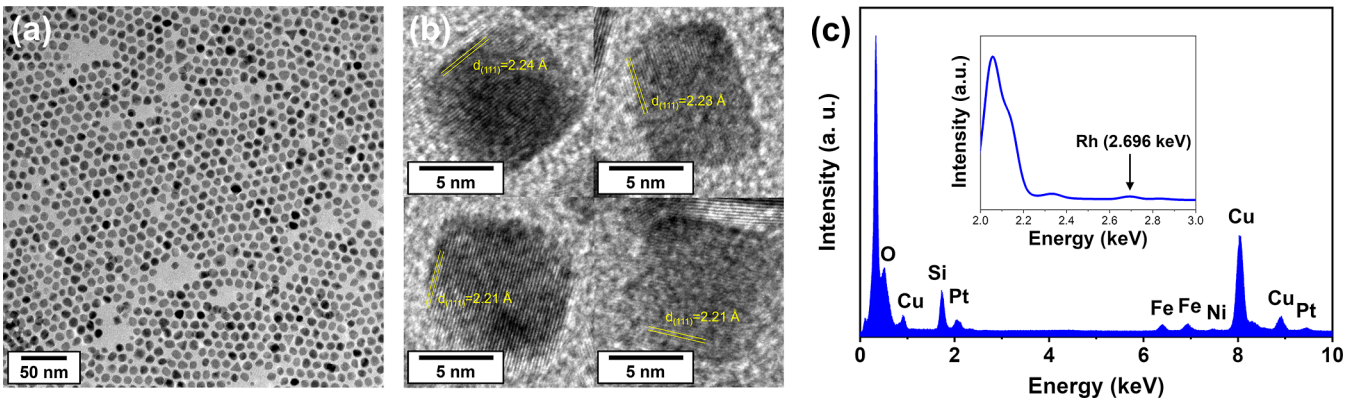

Figure 1. TEM image of the as-synthesized Rh-doped PtNi nanoparticles with (a) low magnification and (b) high magnification. (c) EDS spectra of Rh-doped PtNi nanoparticles (inset: enlarged region with 2−3 keV). Note that the Si peak comes from the detector, while signals of Fe originate from contamination on the detector.

impressive long-term ORR durability, experiencing only a 9.2% reduction in mass activity after 10,000 cycles. We conducted a comprehensive comparison of APT with the conventional STEM-EDS on these nanoparticles to highlight the complementarities. Our analysis delves into the surface chemistry of these nanoparticles, offering potential insights into the impact of trace elements on the catalytic properties of nanoparticles.

RESULTS AND DISCUSSION

The Rh-doped PtNi nanoparticles were first synthesized following the protocol described in ref 26 at room temperature and using high-quality analytical grade chemicals from Sigma-Aldrich. Transmission electron microscopy (TEM) images in Figure 1a reveal the as-synthesized, uniformly shaped octahedral nanoparticles with a size of 8.2 ± 0.8 nm. The longest diameter of 100 randomly selected particles was measured to determine the average particle size. At higher magnification, Figure 1b, sets of {111} planes are imaged with an interplanar distance of 2.22 ± 0.02 Å.[26] STEM-EDS shows 67.2 ± 8.0 at. % Pt and 32.8 ± 8.0 at. % Ni. In earlier investigations on heavily Rh-doped (11 at. %) Pt_3Ni nanoparticles,[26] an accumulation of Rh atoms at the surfaces of the ternary nanoparticles was observed. However, while Pt and Ni peaks were clearly observed in the spectrum in Figure 1c, the Rh-Lα peak at 2.696 eV was barely noticeable.

For APT measurement on nanoparticles, we introduced coelectrodeposition, an enabling versatile approach to embed freestanding nanoparticles in a metallic matrix and facilitate preparation of specimens[29] by focused ion beam milling. Here, the as-synthesized nanoparticles were deposited first by electrophoresis on a pure Co substrate. The residual solution is removed. Scanning electron microscopy (SEM) images of the as-synthesized Rh-doped PtNi nanoparticles deposited on the Co substrate in Figure 2a,b revealed that the nanoparticles remained intact and were not subjected to deformation or corrosion during the electrophoretic process.

After electrophoretic deposition of Rh-doped PtNi nanoparticles, 100 cycles of cyclic voltammetry (CV) between 0 and 1.0 V (vs RHE) in 0.5 M NaOH with a scan rate of 0.5 V s^{-1} were performed on the electrode to remove the ligands used for nanoparticle synthesis.[30] The solution was then substituted with a solution containing Co ions for electroplating to encapsulate the nanoparticles. Pulsed electrodeposition was then carried out to fill the voids between the particles with Co,

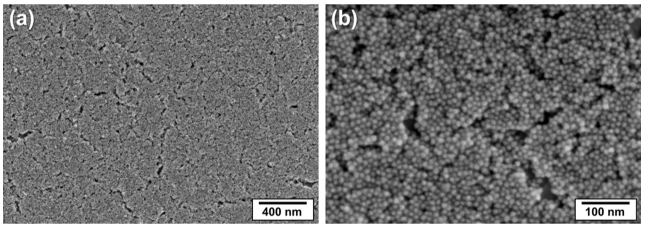

Figure 2. (a,b) SEM images of the anode substrate with electrophoresed Rh-doped PtNi nanoparticles.

using a current of 5 mA for 120 s.[31] Figure 3a shows a cross-sectional STEM image of the encapsulated nanoparticles in the Co film with a high concentration of nanoparticles at the surface of the Co substrate. Based on the elemental mappings in Figure 3b, it appears that no element has undergone galvanic dissolution into the Co matrix during electrodeposition. However, the Rh signal in EDS remained too weak for a precise quantitative analysis. As an indication, the regions with a high particle density comprised 65.5 ± 6.8 at. % Pt, 32.2 ± 0.4 at. % Ni, and 2.4 ± 0.1 at. % Rh.

The APT measurement was performed in the UV-laser mode in 4000 HR LEAP at a base temperature of 45.5 K, a pulsing frequency of 125 kHz, and a detection rate of 0.5%. AP Suite provided by CAMECA was used to reconstruct a data set of 7.3 × 10^6 atoms of Pt, Ni, and Rh obtained from a set of agglomerated nanoparticles, i.e., excluding the Co matrix atoms. Considering an atom detection efficiency of 37% of 4000 HR atom probe model, 2 × 10^5 atoms of Pt, Ni, and Rh elements were collected. Thus, each 8 nm-length octahedral face-centered cubic nanoparticle is calculated to consist of approximately 30,000 atoms, indicating that there are ∼7 nanoparticles in this data set. The 3D atom map of the Rh-doped PtNi nanoparticles embedded in Co is displayed in Figure 4a. The isocompositional surface at 33 at. % Pt (yellow) highlights the interface between the nanoparticle and the matrix, and it is the corner-like shape which suggests an edge of an octahedral nanoparticle based on the result of TEM imaging. Co atoms (shown in blue) are not expected within the nanoparticles; however, the overlap in the mass spectrum between the tail of the main Ni peak and Co makes it difficult to precisely assess (see the Supporting Information). The overall compositions for Pt, Ni, and Rh are 64.8 ± 0.2, 33.5 ± 0.3, and 1.7 ± 0.4 at. %, respectively. Pt and Ni atoms appear randomly distributed in the nanoparticle, whereas Rh atoms,

https://doi.org/10.1021/acs.jpcc.3c05016
J. Phys. Chem. C 2023, 127, 22721−22725

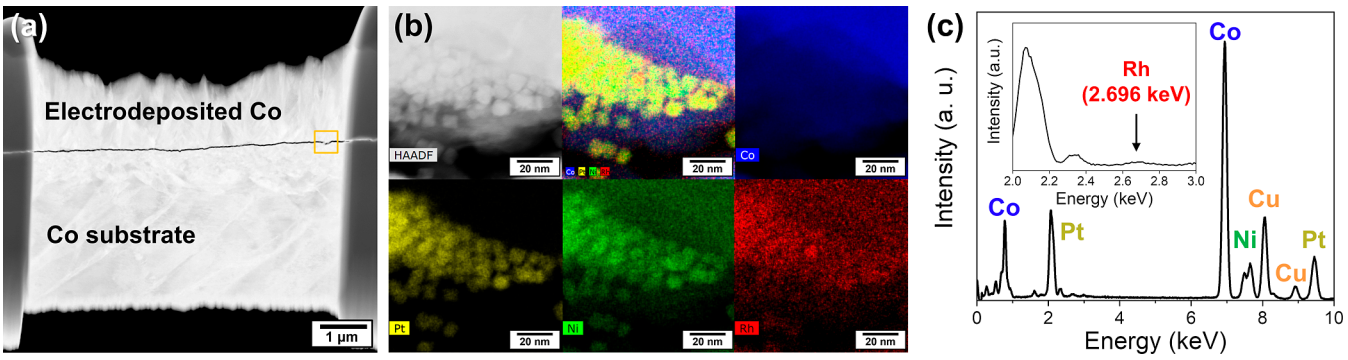

Figure 3. (a) Cross-sectional STEM image after pulsed electrodeposition. (b) EDS mapping and (c) corresponding spectrum of the dense particle zone.

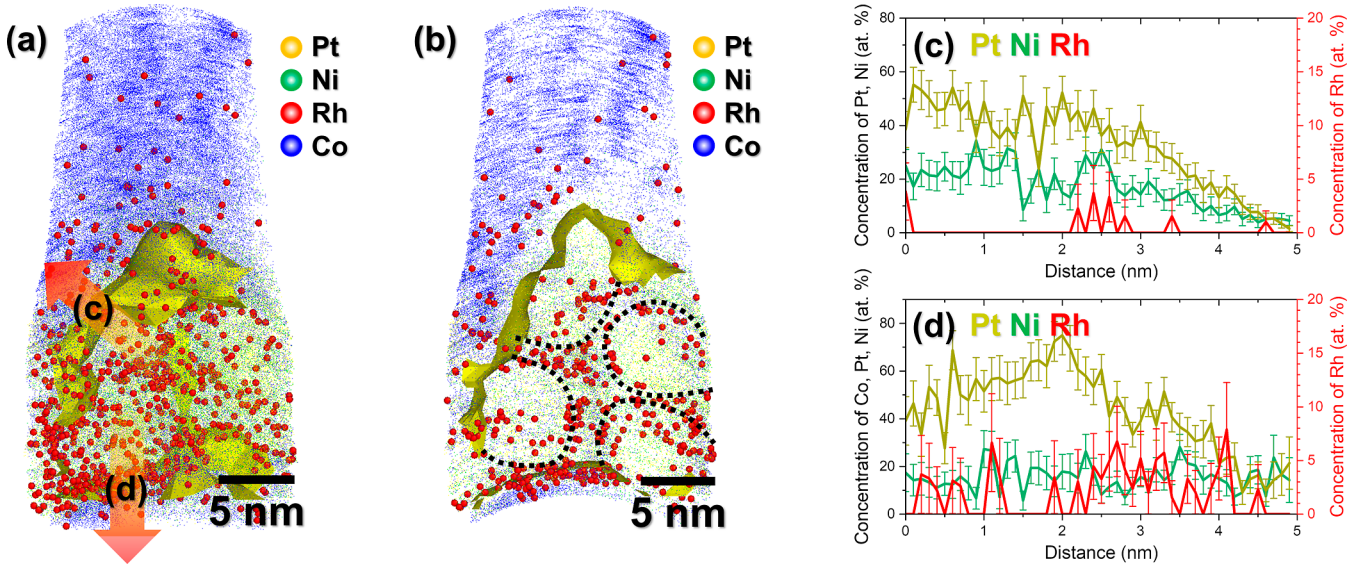

Figure 4. (a) 3D atom map for all the elements including Pt 20 atom % isosurfaces. (b) 3 nm-thin sliced Rh-doped PtNi nanoparticles embedded in Co. Red dots represent the reconstructed Rh atoms, and dotted black lines represent each nanoparticle surface. (c,d) 1D compositional profile ($\phi 5 \times 5$ nm^3) across the interface between Rh-doped PtNi NPs and Co matrix. The qualitative study of Rh segregation is discussed in Figure S2.

which are displayed as red spheres, show a tendency for agglomeration evidenced in the 3 nm slice through the tomogram in Figure 4b. The elemental distribution in the nanoparticles is further quantified by using one-dimensional compositional profiles positioned normally to the surface of individual nanoparticles, Figure 4c,d, indicating up to 4−6 at. % of Rh (red) segregation on the nanoparticles' surfaces.

Challenges in quantifying trace amounts of Rh segregation in ternary nanoparticles have precluded their study, leading to an erroneous assumption that Rh was homogeneously distributed. For instance, Erini et al.[26] studied Pt_3Ni nanoparticles doped with 3 at. % Rh revealing surface segregation of Rh, while in the case of 1 at. % Rh-doped nanoparticles, it was difficult to differentiate the segregation of Rh using STEM-EDS. This finding suggests that it is challenging to assess the degree of surface of bulk segregation below a concentration threshold, here in the range of 3 at. %, i.e., higher than in the particles we synthesized in which we measured 1.7 ± 0.4 at. % Rh by APT.

Recent experiments and computational calculations on bulk Pt−Rh suggest that there is no miscibility gap,[32] contradicting the phase diagram reported by Raub.[33] In nanomaterials, distinct surface segregation of Rh has often been observed in the Pt−Rh system due to external driving forces by surface adsorbents, including O_2 and H_2 from the atmosphere.[34,35] Although the synthesis of the nanoparticle in this study was carried out under a N_2 environment, exposure to air during washing and storage was unavoidable, and this could have triggered surface segregation of Rh. On the contrary to Pt−Rh, the Ni−Rh system has a miscibility gap close to the Rh-rich side of the phase diagram.[36] Surface energy, strain energy, and bond energy induce element segregation of Rh, and Su et al. have demonstrated why the trace amount of Rh is enough to increase the stability for Ni−Rh nanoparticles.[37] Studying how the distribution of minor elements, such as Rh, changes under conditions of oxygen reduction reaction (ORR) could be a promising area of research for future investigations.

CONCLUSIONS

In summary, we synthesized Rh-doped PtNi nanoparticles and revealed that contrary to earlier suggestion that Rh atoms are homogeneously distributed inside the nanoparticles, Rh segregates to the surface. Our finding of evidence that the chemistry of the nanoparticle is more complex than previously reported and investigation of the relationship between composition and catalytic activity (e.g., for the ORR) must be revisited to account for this newly revealed surface chemistry, which will form the basis for future studies.

https://doi.org/10.1021/acs.jpcc.3c05016
J. Phys. Chem. C 2023, 127, 22721−22725

■ ASSOCIATED CONTENT

Data Availability Statement

The data that support the findings of this study are available from the corresponding author upon reasonable request.

Supporting Information

The Supporting Information is available free of charge at https://pubs.acs.org/doi/10.1021/acs.jpcc.3c05016.

Mass spectra of Rd-doped PtNi nanoparticle and nearest-neighbor analyses of reconstructed Rh atoms (PDF)

■ AUTHOR INFORMATION

Corresponding Authors

Se-Ho Kim − *Max-Planck-Institut für Eisenforschung, 40237 Düsseldorf, Germany; Department of Materials Science and Engineering, Korea University, Seoul 02841, Republic of Korea;* orcid.org/0000-0003-1227-8897; Email: sehonetkr@korea.ac.kr

Chanwon Jung − *Department of Materials Science and Engineering, Korea Advanced Institute of Science and Technology (KAIST), Daejeon 34141, Republic of Korea; Max-Planck-Institut für Eisenforschung, 40237 Düsseldorf, Germany;* orcid.org/0000-0002-9782-0261; Email: c.jung@mpie.de

Authors

Hosun Jun − *Department of Materials Science and Engineering, Korea Advanced Institute of Science and Technology (KAIST), Daejeon 34141, Republic of Korea;* orcid.org/0000-0002-1863-1391

Kyuseon Jang − *Department of Materials Science and Engineering, Korea Advanced Institute of Science and Technology (KAIST), Daejeon 34141, Republic of Korea*

Pyuck-Pa Choi − *Department of Materials Science and Engineering, Korea Advanced Institute of Science and Technology (KAIST), Daejeon 34141, Republic of Korea;* orcid.org/0000-0001-9920-0755

Baptiste Gault − *Max-Planck-Institut für Eisenforschung, 40237 Düsseldorf, Germany; Department of Materials, Imperial College London, SW7 2AZ London, U.K.*

Complete contact information is available at: https://pubs.acs.org/10.1021/acs.jpcc.3c05016

Funding

Open access funded by Max Planck Society.

Notes

The authors declare no competing financial interest.

■ ACKNOWLEDGMENTS

This work was supported by the National Research Foundation of Korea (NRF) (grant number 2020R1A6A3A13073143) and was also supported by a Korea University Grant. S.-H.K. acknowledges the KIAT grant funded by the Korea Government MOTIE (P0023676). S.-H.K. and B.G. acknowledge the financial support from the German Research Foundation (DFG) through DIP Project no. 450800666.

■ REFERENCES

(1) O'hayre, R.; Cha, S.-W.; Colella, W.; Prinz, F. B. *Fuel Cell Fundamentals*; John Wiley & Sons, Inc.: Hoboken, NJ, 2016.

(2) Kodama, K.; Nagai, T.; Kuwaki, A.; Jinnouchi, R.; Morimoto, Y. Challenges in Applying Highly Active Pt-Based Nanostructured Catalysts for Oxygen Reduction Reactions to Fuel Cell Vehicles. *Nat. Nanotechnol.* **2021**, *16* (2), 140−147.

(3) Pollet, B. G.; Kocha, S. S.; Staffell, I. Current Status of Automotive Fuel Cells for Sustainable Transport. *Curr. Opin. Electrochem.* **2019**, *16*, 90−95.

(4) Cui, C.; Gan, L.; Heggen, M.; Rudi, S.; Strasser, P. Compositional Segregation in Shaped Pt Alloy Nanoparticles and Their Structural Behaviour during Electrocatalysis. *Nat. Mater.* **2013**, *12* (8), 765−771.

(5) Li, J.; Yin, H.-M.; Li, X.-B.; Okunishi, E.; Shen, Y.-L.; He, J.; Tang, Z.-K.; Wang, W.-X.; Yücelen, E.; Li, C.; et al. Surface Evolution of a Pt-Pd-Au Electrocatalyst for Stable Oxygen Reduction. *Nat. Energy* **2017**, *2* (8), 17111.

(6) Hernandez-Fernandez, P.; Masini, F.; McCarthy, D. N.; Strebel, C. E.; Friebel, D.; Deiana, D.; Malacrida, P.; Nierhoff, A.; Bodin, A.; Wise, A. M.; et al. Mass-Selected Nanoparticles of Pt x Y as Model Catalysts for Oxygen Electroreduction. *Nat. Chem.* **2014**, *6* (8), 732−738.

(7) Sievers, G. W.; Jensen, A. W.; Quinson, J.; Zana, A.; Bizzotto, F.; Oezaslan, M.; Dworzak, A.; Kirkensgaard, J. J. K.; Smitshuysen, T. E. L.; Kadkhodazadeh, S.; et al. Self-Supported Pt-CoO Networks Combining High Specific Activity with High Surface Area for Oxygen Reduction. *Nat. Mater.* **2021**, *20* (2), 208−213.

(8) Jung, C.; Lee, C.; Bang, K.; Lim, J.; Lee, H.; Ryu, H. J.; Cho, E.; Lee, H. M. Synthesis of Chemically Ordered Pt_3Fe/C Intermetallic Electrocatalysts for Oxygen Reduction Reaction with Enhanced Activity and Durability via a Removable Carbon Coating. *ACS Appl. Mater. Interfaces* **2017**, *9* (37), 31806−31815.

(9) Chung, D. Y.; Jun, S. W.; Yoon, G.; Kwon, S. G.; Shin, D. Y.; Seo, P.; Yoo, J. M.; Shin, H.; Chung, Y.-H.; Kim, H.; et al. Highly Durable and Active PtFe Nanocatalyst for Electrochemical Oxygen Reduction Reaction. *J. Am. Chem. Soc.* **2015**, *137* (49), 15478−15485.

(10) Wang, D.; Xin, H. L.; Hovden, R.; Wang, H.; Yu, Y.; Muller, D. A.; DiSalvo, F. J.; Abruña, H. D. Structurally Ordered Intermetallic Platinum-Cobalt Core-Shell Nanoparticles with Enhanced Activity and Stability as Oxygen Reduction Electrocatalysts. *Nat. Mater.* **2013**, *12* (1), 81−87.

(11) Bu, L.; Guo, S.; Zhang, X.; Shen, X.; Su, D.; Lu, G.; Zhu, X.; Yao, J.; Guo, J.; Huang, X. Surface Engineering of Hierarchical Platinum-Cobalt Nanowires for Efficient Electrocatalysis. *Nat. Commun.* **2016**, *7* (1), 11850.

(12) Stamenkovic, V. R.; Fowler, B.; Mun, B. S.; Wang, G.; Ross, P. N.; Lucas, C. A.; Marković, N. M. Improved Oxygen Reduction Activity on Pt3Ni (111) via Increased Surface Site Availability. *Science* **2007**, *315* (5811), 493−497.

(13) Chen, C.; Kang, Y.; Huo, Z.; Zhu, Z.; Huang, W.; Xin, H. L.; Snyder, J. D.; Li, D.; Herron, J. A.; Mavrikakis, M.; et al. Highly Crystalline Multimetallic Nanoframes with Three-Dimensional Electrocatalytic Surfaces. *Science* **2014**, *343* (6177), 1339−1343.

(14) Huang, X.; Zhao, Z.; Cao, L.; Chen, Y.; Zhu, E.; Lin, Z.; Li, M.; Yan, A.; Zettl, A.; Wang, Y. M.; et al. High-Performance Transition Metal-Doped Pt3Ni Octahedra for Oxygen Reduction Reaction. *Science* **2015**, *348* (6240), 1230−1234.

(15) Tian, X.; Zhao, X.; Su, Y.-Q.; Wang, L.; Wang, H.; Dang, D.; Chi, B.; Liu, H.; Hensen, E. J. M.; Lou, X. W.; et al. Engineering Bunched Pt-Ni Alloy Nanocages for Efficient Oxygen Reduction in Practical Fuel Cells. *Science* **2019**, *366* (6467), 850−856.

(16) Lim, J.; Jung, C.; Hong, D.; Bak, J.; Shin, J.; Kim, M.; Song, D.; Lee, C.; Lim, J.; Lee, H.; et al. Atomically Ordered Pt_3Mn Intermetallic Electrocatalysts for the Oxygen Reduction Reaction in Fuel Cells. *J. Mater. Chem. A* **2022**, *10*, 7399−7408.

(17) Kang, Y.; Murray, C. B. Synthesis and Electrocatalytic Properties of Cubic Mn-Pt Nanocrystals (Nanocubes). *J. Am. Chem. Soc.* **2010**, *132* (22), 7568−7569.

(18) Yao, Y.; Huang, Z.; Xie, P.; Lacey, S. D.; Jacob, R. J.; Xie, H.; Chen, F.; Nie, A.; Pu, T.; Rehwoldt, M.; et al. Carbothermal Shock

Synthesis of High-Entropy-Alloy Nanoparticles. *Science* **2018**, *359* (6383), 1489−1494.
(19) Yao, Y.; Dong, Q.; Brozena, A.; Luo, J.; Miao, J.; Chi, M.; Wang, C.; Kevrekidis, I. G.; Ren, Z. J.; Greeley, J.; et al. High-Entropy Nanoparticles: Synthesis-Structure-Property Relationships and Data-Driven Discovery. *Science* **2022**, *376* (6589), No. eabn3103.
(20) Kim, S.-H.; Yoo, S.-H.; Shin, S.; El-Zoka, A. A.; Kasian, O.; Lim, J.; Jeong, J.; Scheu, C.; Neugebauer, J.; Lee, H.; et al. Controlled Doping of Electrocatalysts through Engineering Impurities. *Adv. Mater.* **2022**, *34* (28), 2203030.
(21) Kim, S.; Lim, J.; Sahu, R.; Kasian, O.; Stephenson, L. T.; Scheu, C.; Gault, B. Direct Imaging of Dopant and Impurity Distributions in 2D MoS_2. *Adv. Mater.* **2020**, *32* (8), 1907235.
(22) Jang, K.; Kim, S.-H.; Jun, H.; Jung, C.; Yu, J.; Lee, S.; Choi, P.-P. Three-Dimensional Atomic Mapping of Ligands on Palladium Nanoparticles by Atom Probe Tomography. *Nat. Commun.* **2021**, *12* (1), 4301.
(23) Jung, C.; Jun, H.; Jang, K.; Kim, S.-H.; Choi, P.-P. Tracking the Mn Diffusion in the Carbon-Supported Nanoparticles through the Collaborative Analysis of Atom Probe and Evaporation Simulation. *Microsc. Microanal.* **2022**, *28* (6), 1841−1850.
(24) Carter, C. B.; Williams, D. B. *Transmission Electron Microscopy: Diffraction, Imaging, and Spectrometry*; Springer, 2016.
(25) Kim, H.-K.; Ha, H.-Y.; Bae, J.-H.; Cho, M. K.; Kim, J.; Han, J.; Suh, J.-Y.; Kim, G.-H.; Lee, T.-H.; Jang, J. H.; et al. Nanoscale Light Element Identification Using Machine Learning Aided STEM-EDS. *Sci. Rep.* **2020**, *10* (1), 13699.
(26) Erini, N.; Beermann, V.; Gocyla, M.; Gliech, M.; Heggen, M.; Dunin-Borkowski, R. E.; Strasser, P. The Effect of Surface Site Ensembles on the Activity and Selectivity of Ethanol Electrooxidation by Octahedral PtNiRh Nanoparticles. *Angew. Chem.* **2017**, *129* (23), 6633−6638.
(27) Li, K.; Li, X.; Huang, H.; Luo, L.; Li, X.; Yan, X.; Ma, C.; Si, R.; Yang, J.; Zeng, J. One-Nanometer-Thick PtNiRh Trimetallic Nanowires with Enhanced Oxygen Reduction Electrocatalysis in Acid Media: Integrating Multiple Advantages into One Catalyst. *J. Am. Chem. Soc.* **2018**, *140* (47), 16159−16167.
(28) Beermann, V.; Gocyla, M.; Willinger, E.; Rudi, S.; Heggen, M.; Dunin-Borkowski, R. E.; Willinger, M.-G.; Strasser, P. Rh-Doped Pt-Ni Octahedral Nanoparticles: Understanding the Correlation between Elemental Distribution, Oxygen Reduction Reaction, and Shape Stability. *Nano Lett.* **2016**, *16* (3), 1719−1725.
(29) Kim, S.-H.; Kang, P. W.; Park, O. O.; Seol, J.-B.; Ahn, J.-P.; Lee, J. Y.; Choi, P.-P. A New Method for Mapping the Three-Dimensional Atomic Distribution within Nanoparticles by Atom Probe Tomography (APT). *Ultramicroscopy* **2018**, *190*, 30−38.
(30) Yang, H.; Tang, Y.; Zou, S. Electrochemical Removal of Surfactants from Pt Nanocubes. *Electrochem. Commun.* **2014**, *38*, 134−137.
(31) Jun, H.; Jang, K.; Jung, C.; Choi, P.-P. Atom Probe Tomography Investigations of Ag Nanoparticles Embedded in Pulse-Electrodeposited Ni Films. *Microsc. Microanal.* **2021**, *27*, 1007−1016.
(32) Maisel, S. B.; Kerscher, T. C.; Müller, S. No Miscibility Gap in Pt-Rh Binary Alloys: A First-Principles Study. *Acta Mater.* **2012**, *60* (3), 1093−1098.
(33) Raub, E. Metals and Alloys of the Platinum Group. *J. Less-Common Met.* **1959**, *1* (1), 3−18.
(34) Kawaguchi, T.; Keller, T. F.; Runge, H.; Gelisio, L.; Seitz, C.; Kim, Y. Y.; Maxey, E. R.; Cha, W.; Ulvestad, A.; Hruszkewycz, S. O.; et al. Gas-Induced Segregation in Pt-Rh Alloy Nanoparticles Observed by in Situ Bragg Coherent Diffraction Imaging. *Phys. Rev. Lett.* **2019**, *123* (24), 246001.
(35) Li, T.; Bagot, P. A. J.; Marquis, E. A.; Tsang, S. C. E.; Smith, G. D. W. Characterization of Oxidation and Reduction of Pt-Ru and Pt-Rh-Ru Alloys by Atom Probe Tomography and Comparison with Pt-Rh. *J. Phys. Chem. C* **2012**, *116* (33), 17633−17640.
(36) Nash, A.; Nash, P. The Ni-Rh (Nickel-Rhodium) System. *Bull. Alloy Phase Diagrams* **1984**, *5* (4), 403−405.
(37) Xu, Y.; Wang, G.; Qian, P.; Su, Y. Element Segregation and Thermal Stability of Ni-Rh Nanoparticles. *J. Solid State Chem.* **2022**, *311*, 123096.

https://doi.org/10.1021/acs.jpcc.3c05016
J. Phys. Chem. C 2023, 127, 22721−22725